

Global Cancer Risk from Unregulated Polycyclic Aromatic Hydrocarbons

jamie kelly¹, peter ivatt², Mathew J. Evans³, Jesse H Kroll⁴, Amy Hrdina⁴, ishwar N kohale⁴, forest M white⁴, Bevin P Engelward⁴, and Noelle Eckley Selin¹

¹Massachusetts Institute of Technology

²Unknown

³University of York

⁴MIT

November 24, 2022

Abstract

Scientists and regulators commonly use benzo[a]pyrene concentrations to assess cancer risk from complex mixtures of atmospheric polycyclic aromatic hydrocarbons (PAHs). Here, we show that benzo[a]pyrene is a poor indicator of PAH risk distribution and management: nearly 90% of cancer risk worldwide results from other PAHs, including unregulated degradation products of emitted PAHs. We develop and apply a global-scale atmospheric model and conduct health impact analyses to estimate human cancer risk from 16 PAHs and their N-PAH degradation products. We find that benzo[a]pyrene is a minor contributor to the total cancer risks of PAHs (11%); the remaining risk comes from other directly-emitted PAHs (73%) and N-PAHs (15%). We show that assessment and policy-making that relies solely on benzo[a]pyrene exposure provides misleading estimates of risk distribution, the importance of chemical processes, and the prospects for risk mitigation. We conclude that researchers and decision-makers should consider additional PAHs as well as degradation products.

Hosted file

agu_supplementary_information_2_jmk.docx available at <https://authorea.com/users/550542/articles/604027-global-cancer-risk-from-unregulated-polycyclic-aromatic-hydrocarbons>

Global Cancer Risk from Unregulated Polycyclic Aromatic Hydrocarbons

Jamie M. Kelly^{1,*}, Peter D. Ivatt², Mathew J. Evans^{2,3}, Jesse H. Kroll⁴, Amy I. H. Hrdina⁴,
Ishwar N. Kohale^{5,6}, Forest M. White^{5,6,7}, Bevin P. Engelward⁷, and Noelle E. Selin^{1,8,*}

¹Institute for Data, Systems, and Society, Massachusetts Institute of Technology, MA, 02139, USA.

²Wolfson Atmospheric Chemistry Laboratories, Department of Chemistry, University of York, York, YO10 5DD, UK.

³National Centre for Atmospheric Science, Wolfson Atmospheric Chemistry Laboratories, University of York, YO10 5DD, UK.

⁴Department of Civil and Environmental Engineering, Massachusetts Institute of Technology, Cambridge, MA, 02139, USA.

⁵Department of Biological Engineering, Massachusetts Institute of Technology, Cambridge, MA, 02139, USA.

⁶David H. Koch Institute for Integrative Cancer Research, Massachusetts Institute of Technology, Cambridge, MA, 02139, USA.

⁷Center for Precision Cancer Medicine, Massachusetts Institute of Technology, Cambridge, MA, 02139, USA.

⁸Department of Earth, Atmospheric and Planetary Sciences, Massachusetts Institute of Technology, Cambridge, MA, 02139, USA.

Corresponding authors(*): Jamie M. Kelly (jamiemel@mit.edu) and Noelle E. Selin (selin@mit.edu)

Key Points:

- Benzo[a]pyrene is a small contributor to human cancer risk of PAHs worldwide (11 %)
- Using benzo[a]pyrene as a surrogate compound leads to erroneous conclusions about high-risk populations and the importance of uncertain chemical processes
- Science and policy could be improved by considering a wider group of both emitted PAHs as well as their degradation products

31 Abstract

32 Scientists and regulators commonly use benzo[a]pyrene concentrations to assess cancer risk from
33 complex mixtures of atmospheric polycyclic aromatic hydrocarbons (PAHs). Here, we show that
34 benzo[a]pyrene is a poor indicator of PAH risk distribution and management: nearly 90% of
35 cancer risk worldwide results from other PAHs, including unregulated degradation products of
36 emitted PAHs. We develop and apply a global-scale atmospheric model and conduct health
37 impact analyses to estimate human cancer risk from 16 PAHs and their N-PAH degradation
38 products. We find that benzo[a]pyrene is a minor contributor to the total cancer risks of PAHs
39 (11%); the remaining risk comes from other directly-emitted PAHs (73%) and N-PAHs (15%).
40 We show that assessment and policy-making that relies solely on benzo[a]pyrene exposure
41 provides misleading estimates of risk distribution, the importance of chemical processes, and the
42 prospects for risk mitigation. We conclude that researchers and decision-makers should consider
43 additional PAHs as well as degradation products.

45 Plain Language Summary

46 Nearly 90% of global human lung cancer risk from polycyclic aromatic hydrocarbons (PAHs)
47 comes from compounds omitted by prior analyses and not regulated directly. PAHs in the
48 atmosphere are a complex mixture, but regulators and researchers often represent them using a
49 single compound, benzo(a)pyrene. We show that benzo(a)pyrene is a poor indicator of global
50 PAH cancer risk; its use as a proxy leads to erroneous conclusions about high-risk populations
51 and atmospheric chemical processes. 15% of risk comes from PAHs that are produced in
52 atmospheric reactions and are not regulated or routinely monitored. Regulators and researchers
53 should focus on the entire mixture of PAHs in the atmosphere, and we recommend that
54 benzo(a)pyrene not be used as a sole reference compound.

56 1 Introduction

57 Polycyclic aromatic hydrocarbons (PAHs) are a class of chemicals that contain multiple fused
58 aromatic rings, and are emitted into the atmosphere as byproducts of burning organic matter
59 (Keyte et al., 2013). Several PAHs have been identified as mutagenic or carcinogenic (Bostrom
60 et al., 2002) and therefore have the potential to harm the health of humans (Hansen et al., 2007;
61 Park & Park, 2009) and ecosystems (Gray, 2002). In the atmosphere, PAHs are present as a
62 complex mixture, with different people inhaling different combinations of these carcinogens
63 (Dixon et al., 2019). However, scientific research and environmental guidelines often represent
64 this complex PAH mixture using a single surrogate compound, benzo[a]pyrene (BAP).

65 Epidemiological (Armstrong et al., 2004; Moolgavkar et al., 1998) and animal (Collins et
66 al., 1991; Heinrich et al., 1994; Thyssen et al., 1981) studies have been used to estimate the
67 cancer risk of human exposure to BAP, even though humans are exposed to many different kinds
68 of PAHs. Risk estimates derived from epidemiological studies imply that exposure of 1 ng m^{-3}
69 of BAP to a population of 1 million people will induce 230-830 cancer cases over their lifetime
70 (~70 years). This is equivalent to an epidemiologically-derived unit risk (UR_E) that ranges 213-
71 850×10^{-6} per (ng/m^3) (Armstrong et al., 2004; Moolgavkar et al., 1998). Existing
72 epidemiological studies have not accounted for the confounding exposure to other PAHs, or
73 exposure to other pollutants such as heavy metals, sulphur dioxide and nitrogen oxide. Cancer

74 risks derived from studies in which animals were exposed to BAP alone are lower than those
75 derived from epidemiological studies ($UR_A = 0.3-1.7 \times 10^{-6}$ per (ng/m^3)) (Collins et al., 1991;
76 Thyssen et al., 1981) suggesting an increased risk associated with other components of PAH
77 mixtures.

78 Scientific research and environmental guidelines nearly always use BAP as an indicator
79 for calculating risk from the entire PAH mixture. Shen et al. (2014) and Shrivastava et al. (2017)
80 estimate global-average human lung cancer risks of $20-31 \times 10^{-6}$ by combining global-scale
81 models of BAP in the atmosphere with an epidemiologically-derived BAP unit risk - however,
82 although estimates of UR_E vary by a factor of ~ 4 , both Shen et al. (2014) and Shrivastava et al.
83 (2017) test only the upper limit of this value. By using BAP as the sole indicator, these studies
84 also assume that variations in BAP concentrations reflect proportional variations in risk. While
85 PAHs are regulated as a class of substances, national and international governing bodies also use
86 BAP as an indicator for all species: BAP is the only PAH to have a guideline concentration. In
87 studies where multiple PAHs are considered, BAP is estimated as the major contributor to the
88 cancer risk of PAHs (40-80%)(Delgado-Saborit et al., 2011; Nielsen et al., 1996; Norramit et al.,
89 2005; Zhang et al., 2016; Zhang et al., 2009), but many of those studies do not include highly
90 toxic emitted PAHs (e.g. dibenz[a,h]anthracene), and none include degradation products.

91 Recent work suggests that the atmospheric degradation products of PAHs, such as those
92 containing a nitro group ($-\text{NO}_2$) that we refer to here as N-PAHs, are highly toxic, but their
93 impact on human health remains uncertain. N-PAHs, including both nitro-PAHs (one $-\text{NO}_2$
94 group) and dinitro-PAHs (two $-\text{NO}_2$ groups), can be up to 1,000 times more toxic than their
95 respective parent compound (Wislocki et al., 1986). Laboratory studies have shown that N-PAHs
96 are formed under several different oxidation reactions in the atmosphere (Keyte et al., 2013). N-
97 PAHs have been detected in a variety of environments, from urban(Albinet et al., 2007; Elzein et
98 al., 2019) to remote (Drotikova et al., 2020; Lammel et al., 2017). The chemical formation of N-
99 PAHs in the atmosphere has been simulated in regional-scale (Mulder et al., 2019) and global-
100 scale (Wilson, 2020) atmospheric modelling studies; those studies, however, did not include a
101 key particle-phase reaction with the nitrate radical (NO_3) that laboratory studies suggest could be
102 an extremely efficient source of N-PAHs (Zelenov et al., 2018; Zhang et al., 2014). Furthermore,
103 as prior studies did not perform human health impact assessments, the importance of N-PAHs in
104 the context of human health, as well as in relation to other advancements in this field, are both
105 unknown.

106 Researchers in previous studies have argued that uncertainties in heterogeneous oxidation
107 kinetics (Poschl et al., 2001; Zhou et al., 2019; Zhou et al., 2013) and gas-particle partitioning
108 (Dachs & Eisenreich, 2000; Shahpoury et al., 2016) have a large effect on exposure and human
109 health impacts of BAP, but the importance of these uncertain processes in the context of other
110 emitted PAHs and degradation products remains unknown. Shrivastava et al. (2017) found that
111 reducing the rate of BAP heterogeneous oxidation resulted in a four-fold increase in estimated
112 human exposure to BAP, and a five-fold increase in PAH human cancer risk when using BAP as
113 an indicator of health risks. However, reductions in the oxidation rate will also diminish human
114 exposure to degradation products, which may themselves be toxic – this effect was not
115 considered by Shrivastava et al. (2017), who used BAP concentrations as a proxy for overall
116 PAH exposure and risk. Additional studies (Friedman et al., 2014; Friedman & Selin, 2012;
117 Friedman et al., 2014; Mu et al., 2018; Thackray et al., 2015) have advanced understanding of
118 PAH chemistry in the atmosphere through simulations of 1-3 PAH species. The sensitivity of

119 process-based conclusions to the inclusion of additional PAHs and degradation products remains
120 unassessed.

121 Here, we reevaluate the importance of BAP and its suitability as an indicator compound
122 for global-scale cancer risk of PAHs, and we perform a bounding exercise to assess how
123 uncertainties in concentrations and atmospheric processes affect conclusions drawn in previous
124 studies which were based on BAP alone. To do this, we develop and use a global-scale
125 atmospheric chemistry model to estimate concentrations of PAHs in the atmosphere, and use
126 human health impact analyses to estimate the human cancer risk associated with atmospheric
127 PAHs, using traditional epidemiologically-based functions as well as a novel framework based
128 on toxicity data from animal studies which allows us to explicitly estimate the risks of individual
129 components of the PAH mixture. In contrast to previous global-scale modeling studies which
130 typically considered only BAP (Friedman et al., 2014; Friedman & Selin, 2012; Friedman et al.,
131 2014; Lammel et al., 2009; Mu et al., 2018; Octayiani et al., 2019; Shen et al., 2014; Shrivastava
132 et al., 2017; Thackray et al., 2015), we account for the 16 PAHs identified as priority pollutants
133 by the United States Environmental Protection Agency (“USEPA16”) as well as N-PAH
134 degradation products. We quantify the sensitivity of estimates of global cancer risk to (i)
135 inclusion of additional PAHs, (ii) gas-particle partitioning, (iii) heterogeneous oxidation kinetics,
136 and (iv) model resolution. We conclude that BAP accounts for only a small fraction of the
137 human cancer risk of PAHs globally, while the N-PAHs, which are unregulated and commonly
138 omitted by measurement and modeling studies focused on the atmosphere, are a potentially large
139 source of carcinogenic risk. We also find that atmospheric kinetic and partitioning uncertainties
140 have a much lower impact on risk magnitudes than was identified in previous studies. We
141 suggest that future research and regulatory guidelines explicitly consider a broader range of
142 PAHs and their degradation products in assessments of cancer risk from these compounds.

143

144 **2 Materials and Methods**

145

146 2.1 Experimental Design

147 We provide a total of fourteen estimates of global human cancer risk from PAHs by combining
148 seven different PAH concentration distributions from a global-scale atmospheric chemistry
149 model, with two distinct methods for estimating human cancer risk. Together, this analysis
150 allows us to quantify the suitability of BAP as an indicator of risk of PAH mixtures, and to
151 bound the importance of contributors to uncertainty.

152

153 2.2 Description of Atmospheric Chemistry Model (GOES-Chem)

154 We use a numerical, three-dimensional, atmospheric chemistry model, GEOS-Chem (Bey et al.,
155 2001; <http://acmg.seas.harvard.edu/geos/>) version 11. We perform model simulations at a two
156 different horizontal resolutions, of 4° x 5° and 2° x 2.5° – both with 47 vertical levels, extending
157 from the surface of the Earth to ~80 km altitude. Meteorological fields are driven by MERRA-2
158 reanalysis from the NASA Global Modeling and Assimilation Office (Global Modeling and

159 Assimilation Office, GMAO). We use the “tropchem” chemical mechanism (Eastham et al.,
160 2014) for this work, which includes a detailed and fully coupled treatment of HO_x –NO_x –VOC–
161 O₃ and a bulk aerosol scheme with fixed log-normal modes. Aerosol components considered
162 include sulfate, sea salt, black carbon, mineral dust and organic carbon. Inorganic aerosol
163 thermodynamics are calculated using ISORROPIA (Fountoukis & Nenes, 2007). Both OC and
164 BC are further separated into hydrophilic and hydrophobic components. The tropchem
165 mechanism is expanded to also consider PAHs (described below – 2.3). Dry deposition of both
166 gases and aerosol are parameterized in a scheme which applies a resistance-in-series approach
167 (Wesely, 1989; Zhang et al., 2001). Wet deposition occurs both within and below clouds, and is
168 dependent on the species-specific effective Henry’s Law constant (Amos et al., 2012). These
169 model simulations use a variety of different global and regional-scale emission inventories for
170 non-PAH species. Global-scale emission inventories used here for non-PAH species include
171 EDGAR (Crippa et al., 2018) and RETRO (Hu et al., 2015). Where necessary, these global-scale
172 emission inventories are overwritten with regional-scale emission inventories - e.g. NEI over
173 USA (Travis et al., 2016), EMEP over Europe (van Donkelaar et al., 2008). For biomass burning
174 and biogenic emissions, we use GFED4 (Giglio et al., 2013) and MEGAN (Guenther et al.,
175 2012), respectively. Emissions of PAHs are discussed in greater detail in the following section.
176 In the next sections, we describe how PAHs are simulated within the GEOS-Chem model,
177 highlighting new developments.

178

179 2.3 Treatment of PAHs and N-PAHs in GEOS-Chem

180 The GEOS-Chem model has previously been used to examine PAH chemistry and transport in
181 the atmosphere, both for the present day (Friedman et al., 2014; Friedman & Selin, 2012;
182 Thackray et al., 2015) and future climate simulations (Friedman et al., 2014). We extend the
183 model (Friedman & Selin, 2012) such that PAHs are now fully interactive with other
184 atmospheric species. This allows a two-way chemical feedback between PAHs and all other
185 gaseous and aerosol species. Previous simulations used an offline version of the model, whereby
186 gas and aerosol concentrations from the ‘full’ chemistry simulation were archived and used as
187 input for the PAH simulation.

188 Whereas previous modelling studies only consider between 1 and 3 PAHs, we extend the
189 GEOS-Chem model to provide global-scale concentration information for a total of 48 PAH
190 species. This consists of 16 emitted PAHs; the US EPA’s list of priority PAHs. These include
191 naphthalene (NAP), acenaphthylene (ACY), acenaphthene (ACE), fluorene (FLU), phenanthrene
192 (PHEN), anthracene (ANT), fluoranthene (FLA), pyrene (PYR), benzo[a]anthracene (BAA),
193 chrysene (CHR), benzo[b]fluoranthene (BBF), benzo[k]fluoranthene (BKF), benzo[a]pyrene
194 (BAP), benzo[g,h,i]perylene (BGHIP), indeno[1,2,3-c,d]pyrene (ICDP), and
195 dibenz[a,h]anthracene (DAHA). The remaining 32 PAH species are the corresponding nitro-
196 PAHs (x16) and dinitro-PAHs (x16).

197 Although commonly neglected from atmospheric modelling studies, we account for N-
198 PAH formation in the atmosphere by building a chemical mechanism. We build a degradation
199 mechanism of pyrene (PYR) that accounts for the formation of nitropyrene (nitro-PYR) and
200 dinitropyrene (dinitro-PYR) (Table 1). This mechanism is generalized, as it is based on the

201 findings from laboratory studies which are not all on pyrene. We chose pyrene for three reasons.
 202 First, pyrene is the only species where N-PAH formation yields have been determined in
 203 laboratory studies for each reaction pathway. Second, N-PYR is included in multiple field
 204 campaigns, allowing us to evaluate our predicted concentrations for this species. Many other N-
 205 PAHs have not been measured in the atmosphere. Third, the toxicity of N-PYR and DN-PYR are
 206 known, allowing us to quantify the human cancer risk of the oxidation products. The mechanism
 207 that describes the source and sinks for pyrene and its N-PAHs is displayed in Table 1. For this
 208 species, we account for the formation of nitropyrene via (i) gas-phase photooxidation, (ii) gas-
 209 phase direct nitration, and (iii) particle-phase direct nitration. Photolysis of the N-PYRs is also
 210 accounted for. For the remaining 15 emitted PAHs, the chemical mechanism only accounts for
 211 the chemical removal of the parent compound, and not the production of the N-PAHs. For these
 212 PAHs, we account for the major sinks (gas-phase photooxidation and particle-phase ozonolysis),
 213 without directly tracking the products of chemical mechanism online in GEOS-Chem. This way
 214 of representing PAHs (i.e. the processes considered, and the neglect of oxidation products), is
 215 consistent with previous global and regional scale modelling studies (e.g. Friedman et al.
 216 (2012)). N-PAH concentrations from these 15 emitted PAHs are estimated in our bounding
 217 exercise and uncertainty analyses by applying the spatial distributions in the N-PYR/PYR and
 218 DN-PYR/PYR ratios (Figure S2, SI) to concentrations of the remaining PAHs as a proxy for
 219 spatial patterns of their N-PAH products.

220

221 **Table 1.** Reaction kinetics for N-PAHs. Chemical and photolytic reactions of pyrene (PYR)
 222 included in the updated version of the chemical-transport model (GEOS-Chem).

	Reaction	2 nd order rate coefficient	Reference
Pyrene (PYR)	Gas-phase		
	R1.	$\text{PYR}_{(g)} + \text{NO}_3 \rightarrow \text{NPYR}$	$1.6 \times 10^{-27} \times [\text{NO}_2]$ (Atkinson et al., 1990; Keyte et al., 2013)
	R2.	$\text{PYR}_{(g)} + \text{OH} \rightarrow \text{PYR-OH}$	5.0×10^{-11} (Atkinson et al., 1990)
	R3.	$\text{PYR-OH} + \text{O}_2 \rightarrow \text{products}$	1.0×10^{-17} (Koch et al., 2007) (from benzene)
	R4.	$\text{PYR-OH} + \text{NO}_2 \rightarrow \text{NPYR}$	3.6×10^{-11} (Feilberg et al., 1999) (from naphthalene)
	Particle-phase		
	R6.	$\text{PYR}_{(p)} + \text{NO}_3 \rightarrow \text{NPYR}$	6.4×10^{-12} (Liu et al., 2012)
R7.	$\text{PYR}_{(p)} + \text{O}_3 \rightarrow \text{products}$	4.27×10^{-17} Mean = (Liu et al., 2012) and (Perraudin et al., 2007)	
Nitropyrene (NPYR)	Gas-phase		
	R8.	$\text{NPYR}_{(g)} + \text{NO}_3 \rightarrow \text{DNPYR}$	$1.6 \times 10^{-27} \times [\text{NO}_2]$ Identical to PYR
	R9.	$\text{NPYR}_{(g)} + \text{OH} \rightarrow \text{NPYR-OH}$	5.0×10^{-11} Identical to PYR
	R10.	$\text{NPYR-OH} + \text{O}_2 \rightarrow \text{products}$	1.0×10^{-17} (Koch et al., 2007) (from benzene)

	R11.	$\text{NPYR-OH} + \text{NO}_2 \rightarrow \text{DNPYR}$	3.6×10^{-11}	(Feilberg et al., 1999) (from naphthalene)
	Particle-phase			
	R12.	$\text{NPYR}_{(p)} + \text{NO}_3 \rightarrow \text{DNPYR}$	1.3×10^{-12}	(Liu et al., 2012)
	R13.	$\text{NPYR}_{(p)} + \text{O}_3 \rightarrow \text{products}$	2.2×10^{-17}	(Miet et al., 2009)
	R14.	$\text{NPYR}_{(p)} + h\nu \rightarrow \text{products}$	$1.3 - 5.0 \times 10^{-4}$	
Dinitropyrene (DNPYR)	Gas-phase			
	R15.	$\text{DNPYR}_{(g)} + \text{NO}_3 \rightarrow \text{products}$	5.0×10^{-11}	Identical to PYR
	R16.	$\text{DNPYR}_{(g)} + \text{OH} \rightarrow \text{products}$	$1.6 \times 10^{-27} \times [\text{NO}_2]$	Identical to PYR
	Particle-phase			
	R17.	$\text{DNPYR}_{(p)} + \text{NO}_3 \rightarrow \text{products}$	1.3×10^{-12}	Same as nitro-PYR
	R18.	$\text{DPYR}_{(p)} + \text{O}_3 \rightarrow \text{products}$	2.2×10^{-17}	Same as nitro-PYR
R19.	$\text{DPYR}_{(p)} + h\nu \rightarrow \text{products}$	$1.3 - 5.0 \times 10^{-4}$		

223

224 We provide two descriptions for heterogeneous oxidation kinetics which differ only by
225 their reaction rate coefficients, allowing us to quantify how uncertainty in the rate of this process
226 contributes to uncertainty in PAH distributions and human cancer risk. Within the GEOS-Chem
227 model, particle-phase ozonolysis kinetics follow the Arrhenius equation using a second-order
228 rate coefficient (k) from Perraudin et al. (2007). Although alternative laboratory studies show
229 that heterogeneous PAH oxidation follows a Langmuir-Hinshelwood type reaction mechanism,
230 implying that k is variable (dependent on ozone), the parameters required to account for these
231 more realistic descriptions of heterogeneous PAH oxidation kinetics have only been developed
232 for a limited number of PAHs, and are not implemented in this study. However, as we know this
233 process could be much slower, we conduct a sensitivity simulation where k is reduced to 10 % of
234 its laboratory-derived value.

235 We implement two widely-used approaches to estimate gas-particle partitioning, allowing
236 us to bound the importance of uncertainties associated with this process. PAHs are semi-volatile,
237 meaning they can partition between gas and particle phases. In the particle-phase, PAHs are
238 observed to either be absorbed within organic aerosol (OA), or adsorbed onto the surface of
239 black carbon (BC). We chose to implement a poly parameter linear free energy (Shahpoury et al.,
240 2016) (ppLFFER) scheme, but for comparison, we also conduct simulations using a single
241 parameter scheme following Dachs and Eisenreich (Dachs & Eisenreich, 2000) (D&E).

242 PAH emissions for the year 2014 are from the global-scale emission inventory developed
243 by Shen et al. (2013). This emission inventory is used widely across global-scale atmospheric
244 modelling studies (Friedman et al., 2014; Friedman & Selin, 2012; Mu et al., 2018; Shrivastava
245 et al., 2017; Thackray et al., 2015). The combined USEPA16 global-total annual-total emission
246 rate is 504 Gg a^{-1} , with an interquartile range of $331\text{-}818 \text{ Gg a}^{-1}$ (Shen et al., 2013) The sectors
247 included in this inventory are residential and commercial, industry, transportation, deforestation,
248 agriculture, and energy production.

249 Gas-phase PAHs undergo dry and wet deposition in a similar fashion to other gases. For
250 all gas-phase species, we assign a Henry's Law solubility constant of $3.1 \times 10^{-5} \text{ m}^3 \text{ atm}^{-1} \text{ mol}^{-1}$,
251 taken from Sander (2015) (Sander, 2015). Particle-phase PAHs are assumed to undergo dry and
252 wet deposition according to the aerosol that it is bound to – that is, dry and wet deposition
253 parameters describing the aerosol particle are used to describe deposition of the particle-phase
254 PAH.

255

256 2.4 GEOS-Chem Model Simulations Performed in Study

257 We perform four global-scale model simulations, which are presented in Table 2. For all
258 simulations, we discard the first month of simulation as spin up, and base our analysis on the
259 remaining 12 months: January 2014 – December 2014. For the base simulation, we use $4^\circ \times 5^\circ$
260 horizontal resolution, second order rate coefficients describing heterogeneous oxidation kinetics
261 are taken directly from the laboratory studies, and gas-particle partitioning follows the ppLFFER
262 scheme. We then perform three sensitivity simulations, where we change one parameter at a

263 time, allowing us to isolate the importance of uncertainties in each of these processes. In the first
 264 sensitivity simulation, we reduce the heterogeneous oxidation rate coefficient to 10 % of its
 265 original value ('Het_0.1'; Table 2). In the second sensitivity simulation, we change the gas-
 266 particle partitioning scheme from the ppLFFER to the D&E scheme ('D&E'; Table 2). In the third
 267 sensitivity simulation, we change the model horizontal resolution from 4° x 5° to 2° x 2.5°
 268 horizontal ('2x2.5'; Table 2).

269

270 **Table 2.** Overview of GEOS-Chem model simulations performed in in this study. Note, whereas
 271 the first four simulations in table are unique model simulations, the final three simulations are
 272 based on the Base simulation, but with various bias-correction techniques applied.

Simulations	Gas-particle partitioning	Gas-particle partitioning scheme	Resolution	Bias-correction
Base	Laboratory-derived	ppLFFER	4° x 5°	None
Het_0.1	10 % of laboratory value	ppLFFER	4° x 5°	None
D&E	Laboratory-derived	D&E	4° x 5°	None
2x2.5	10 % of laboratory value	ppLFFER	2° x 2.5°	None
PAH_Corr	Laboratory-derived	ppLFFER	4° x 5°	Corrected to PAH concentrations from
N-PAH_Min	Laboratory-derived	ppLFFER	4° x 5°	Corrected to minimum N-PAH yields
N-PAH_Max	Laboratory-derived	ppLFFER	4° x 5°	Corrected to maximum N-PAH yields

273

274 2.5 Observations Used to Evaluate Simulated PAHs and Provide Simple Bias-Corrections

275 We use observations to evaluate performance of the four aforementioned GEOS-Chem model
 276 simulations, and also to provide three additional 'bias-corrected' PAH concentration
 277 distributions (from the Base simulation.) Observations for Europe and North America were taken
 278 from continuously-monitoring air quality networks Environmental Protection Agency, Air
 279 Toxics and the European Monitoring and Evaluation Programme (EMEP) (accessed via the
 280 Norwegian Institute for Air Research) and those for continental Asia (Saha et al., 2017), Asia-
 281 Arctic ship cruise transect (Ma et al., 2013), and Africa (Klánová et al., 2008) are from field
 282 campaigns. We apply three different 'bias corrections' to the PAH distributions from the base
 283 simulation. To test for the effects of a bias in the differences in concentrations across the
 284 different PAHs, we multiplied the simulated PAH concentrations by the average bias between
 285 the simulated and observed mean PAH concentration across the non-urban sites (these bias-
 286 correction factors are shown in Table S2, SI). To test for potential biases in simulated N-
 287 PAH/PAH yields, we scaled the model-derived N-PAH/PAH ratio by the maximum/minimum

288 bias between the simulated and observed N-PAH/PAH (these scaling factors are shown in Table
289 S3, SI). This provided upper and lower bound estimates for N-PAH formation potential.

290

291 2.6 Calculation of Incremental Lifetime Cancer Risk

292 We estimate the incremental lifetime cancer risk using two different methods. We combine these
293 methods with PAH distributions from the four model simulations and three bias corrected model
294 simulations, leading to a total of fourteen different estimates of ILCR.

295 In the epidemiologically-based method, we estimate ILCR (unitless) following

$$ILCR = UR_E \times [BAP]$$

296 Where UR_E is the epidemiologically-derived BAP unit-risk (unit = per (ng/m³)), which is
297 estimated at 21.3 (Moolgavkar et al., 1998), 32.7 (Armstrong et al., 2004), 85.0 (Armstrong et
298 al., 2004) $\times 10^{-6}$ per (ng/m³), and [BAP] is the atmospheric concentration (ng/m³) of BAP, which
299 is derived from the model. Under this method, overall ILCR is assumed to scale directly with
300 BAP concentrations, and the impacts of the entire PAH mixture are accounted for (but the
301 mixture is assumed to be fixed across the world).

302 We also develop an animal-based method for estimating ILCR, which allows us to
303 compare the human cancer risk of individual PAH species without double counting. This is
304 calculated following

$$ILCR = \sum UR_A \times [PAH] \times TEQ$$

305 Where UR_A is the animal-derived BAP unit risk (unit = per (ng/m³)), which is estimated
306 estimated by Collins et al., (1991) at 0.37 1.0, or 1.7×10^{-6} per (ng/m³), [PAH] is the atmospheric
307 concentration (ng/m³) of PAHs, and TEQ are their toxic equivalent quotients (unitless). Where
308 possible, we use estimates of TEQ from the primary literature, which have not been rounded to
309 the nearest significant figure or order of magnitude, as is the case in many literature reviews; this
310 rounding would introduce additional uncertainty in the relative importance of different PAHs.
311 However, where the primary literature is not available, we use the recommended values from the
312 literature reviews. TEQ used in this study from the literature are shown in Table 3. We use the
313 terms TEQ and Relative Potency Factor (RPF) interchangeably. This method assumes that the
314 cancer risk of individual PAHs combines linearly, as there is no conclusive evidence to suggest
315 otherwise. This animal-based method only includes the cancer risk of PAHs for which both
316 exposure concentrations and toxicity information were available (28 of the 48 species: all 16
317 emitted of the emitted PAHs, 6 out of the 16 nitro-PAHs, and 6 out of the 16 dinitro-PAHs).
318 When attributing ILCR to different PAHs in the animal-based method, we also account for
319 possible biases in the simulated distribution of PAHs (i.e. differences in concentrations among
320 different PAH species). To account for the effect of possible biases, we used the ‘bias-corrected’
321 spatial distributions of PAHs concentrations (see Table S1 in the SI for scaling factors). We also
322 test for any biases in our predicted N-PAH/PAH ratios by performing sensitivity calculations,
323 where these ratios are scaled using observed values (see Table S2 in the SI for scaling factors).

324 In the two equations above, the unit for the ILCR is cancer risk, and therefore
 325 dimensionless. We can combine these risks with gridded human population density and assume a
 326 human lifetime of 70 years to express the ILCR in the form of cancer rates per year. Gridded
 327 human population density is taken from the Socioeconomic Data and Applications Center
 328 (SEDAC).

329 Across both methods for estimating ILCR, we test minimum, median and maximum
 330 values of BAP toxicity (UR) from the literature. We also used both the epidemiological and
 331 animal-based methods to evaluate how uncertainties in heterogeneous oxidation kinetics affect
 332 estimates of PAH cancer risk, by applying them to two model simulations which differ in the
 333 reactivity of particle-phase PAHs. In the discussion, we provide a more detailed evaluation of
 334 advantages and disadvantages in the epidemiological- and animal-based methods for estimating
 335 ICRL.

336
 337

338 **Table 3.** Relative toxicity of PAHs (TEQ). These values are used in the animal-based method for
 339 estimating ILCR. Note, we use the terms TEQ and RPF interchangeably. a = Nisbet & Lagoy
 340 (1992), b = Busby et al. (1989), c = Wislocki et al. (1986), d = Deutschwenzel et al. (1983), e =
 341 Fu et al. (1998), f = EPA (2009).
 342

	PAH	Nitro-PAH	Dinitro-PAH
NAP	0.001 ^a		
ACY	0.001 ^a		
ACE	0.001 ^a		
FLO	0.00075 ^a		
PHE	0.00075 ^a		
ANT	0.155 ^a		
FLA	0.052 ^b	0.13 ^b	0.13 (assumed)
PYR	0.065 ^c	0.1 ^c	5.1 ^c
BAA	0.35 ^c	0.1 ^c	0.1 (assumed)
CHR	0.011 ^b	10.8 ^c	10.8 (assumed)
BBF	0.210000		
BKF	0.03 ^d		
BAP	-	0.47 ^c	0.47 (assumed)
ICDP	0.08 ^d		
DAHA	3.0 ^e		
BGHIP	0.01 ^{f,b}		

343

344 **3 Results**

345

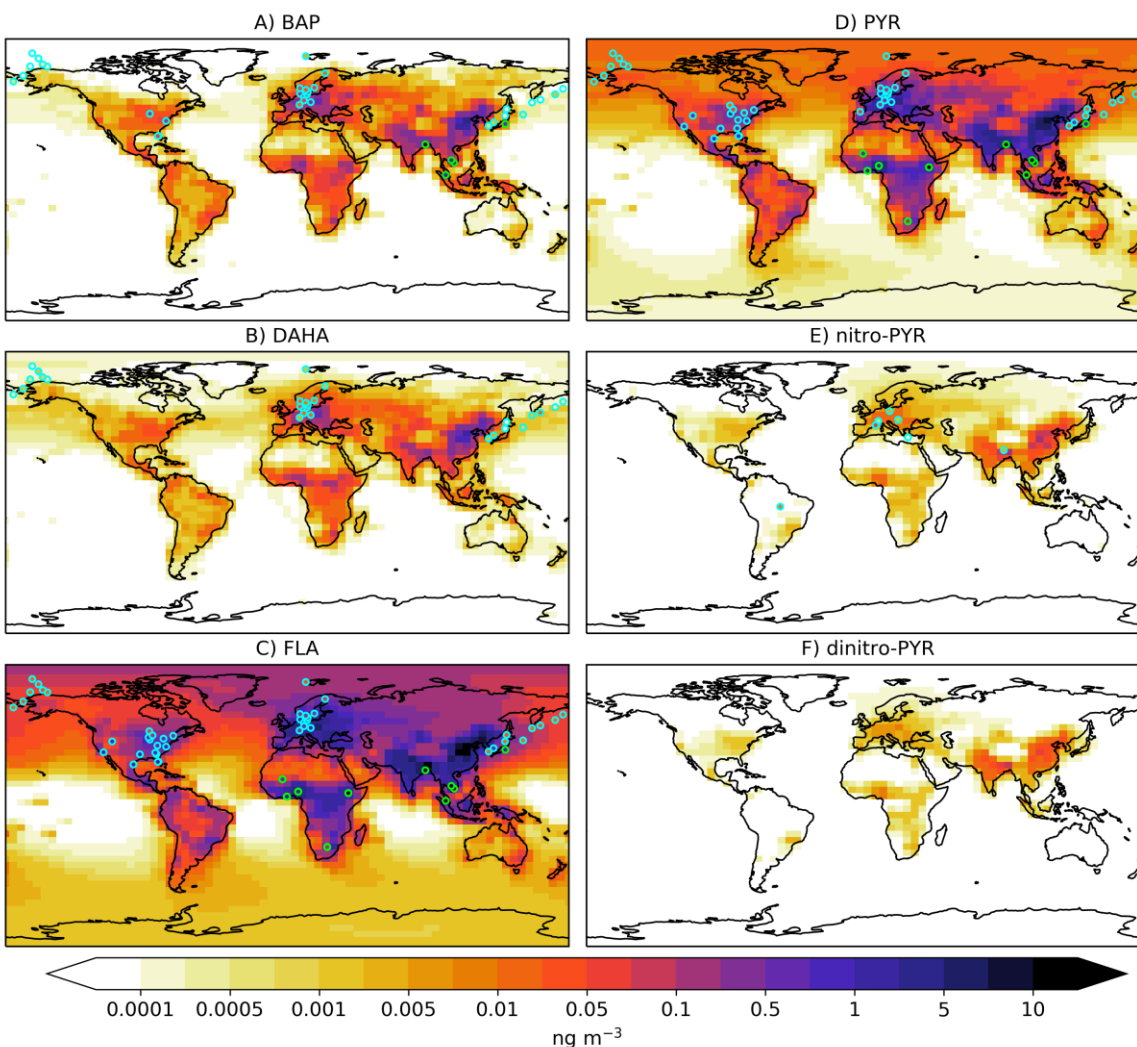
346 3.1 Global and Regional Concentrations of Emitted PAHs

347 We evaluate model performance of simulating 16 emitted PAHs by comparing simulated and
348 observed PAH concentrations in a variety of environments. Simulated PAH concentrations were
349 compared to a variety of different measurements and are displayed in Figures 1. In Figure 1, the
350 simulated annual average surface concentrations for three illustrative PAHs are shown, and
351 observed values are overlaid (circles). The left column shows three emitted PAHs, which are
352 discussed in this section. The right column shows an emitted PAH and the N-PAHs degradation
353 products, which are discussed in the next section.

354 Global PAH simulations are poorly constrained by available data, and many uncertainties exist in
355 their emissions and atmospheric chemistry that affect the ability to model them accurately (see
356 *Global Model Performance* in SI for more detail). As noted in Section 2.6, observations for
357 Europe and North America were taken from continuously-monitoring air quality networks (EPA
358 and EMEP) and those for continental Asia (Saha et al., 2017), Asia-Arctic ship cruise transect
359 (Ma et al., 2013), and Africa (Klánová et al., 2008) are from field campaigns. Simulated and
360 observed data at the location of measurements in Figure 1 are also represented in the form of box
361 and whisker plots (Figure 2), where red reflects observed data, green reflects our base
362 simulation, and blue shows a sensitivity simulation to test the influence of chemical uncertainties
363 (described below). In Figure 2, PAH species on the x-axis are ordered from lowest molecular
364 weight (left) to highest molecular weight (right). A summary of statistics are also shown in the SI
365 (Table S1).

366 The model captures average PAH concentrations for most PAHs, but with some low
367 biases, especially in urban areas. For 11 out of 16 emitted species, the p-value is less than 0.05
368 (indicated by * in Figure 2). Overall, simulated PAH concentrations are lower than observed
369 (Figure 2B). For 13 of the emitted species, the model underpredicts the observed global average
370 PAH concentration (normalized mean bias (NMB) ranges from -97 to -42 %; Figure 2B). For the
371 remaining 3 emitted species (ACY, BKF and DAHA) the model overestimates the observed
372 global-average PAH concentration (NMB = 104 to 464 %; Figure 2B). For non-urban sites (i.e.
373 outside of cities), simulated PAH concentrations are lower than observed over the United States,
374 and higher than observed over Europe. The bias over the US is likely a result of our choice of
375 emission inventory: higher-resolution regional-scale emission inventories predict 2-3 times
376 higher PAH emissions over the US (Zhang et al., 2017) compared to the global-scale emission
377 inventory used in this study (Shen et al., 2013). Similar to other global-scale models (Friedman
378 & Selin, 2012), our simulation underpredicts the high observed PAH concentrations typical of
379 urban environments (Figure 1A-C; green circles), especially in cities across Asia and Africa. In
380 remote regions, the model reproduces heavier molecular weight species measured across a ship
381 cruise from Beijing (CH) to the Arctic (Ma et al., 2013), but underpredicts concentrations of
382 lighter molecular weight species. In Svalbard (Norway), however, the model captures annual
383 average PAH concentrations for the lighter molecular weight species, but underpredicts the

384 heavier molecular weight species by up to several orders of magnitude. Our model performance
 385 at capturing observed BAP concentrations is comparable to that of previous global-scale
 386 modelling studies (see discussion in the SI - *Global Model Performance*).

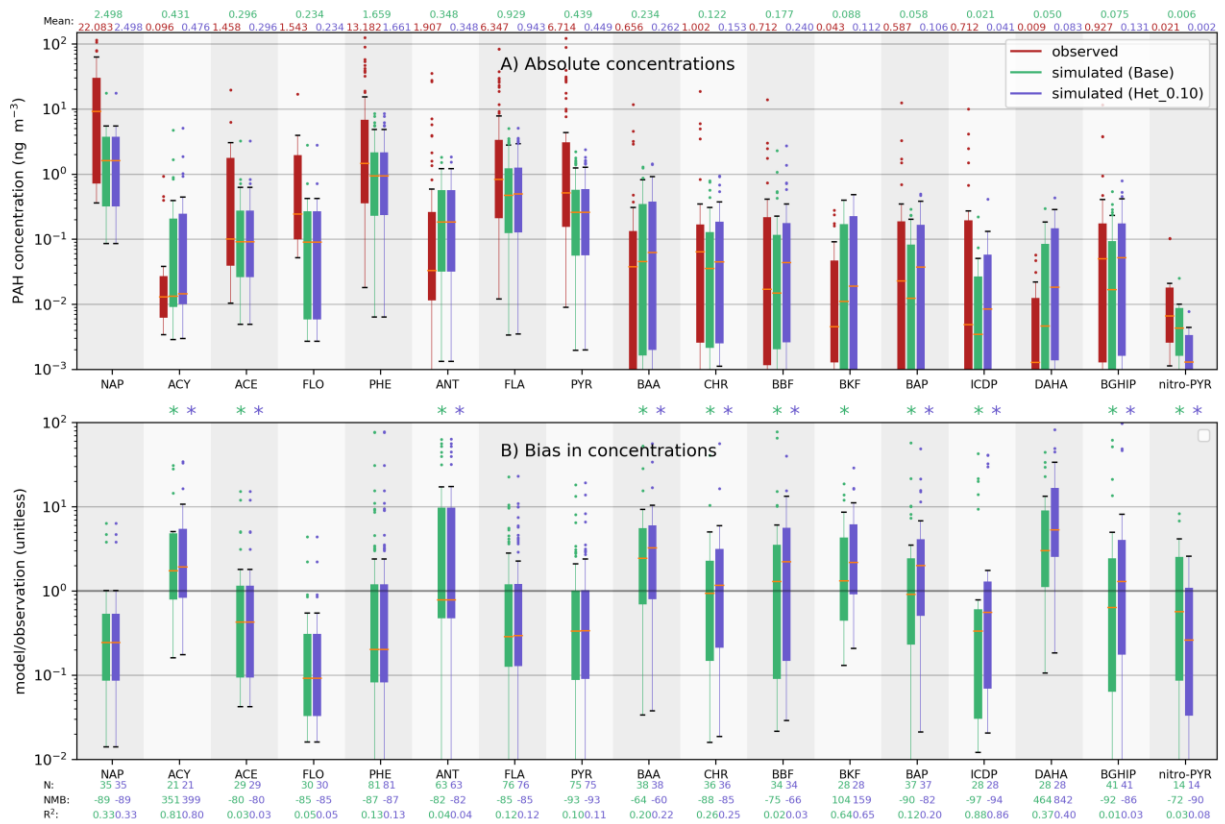


387
 388 **Figure 1.** Spatial distributions of annual-average surface PAH concentrations (ng m⁻³) in the
 389 GEOS-Chem model and overlaid with observed values. The left column shows three emitted
 390 PAHs: A) benzo[a]pyrene (BAP), B) dibenzo[a,h]anthracene (DAHA), and C) f fluoranthene
 391 (FLA). The right column shows a parent compound and its N-PAH degradation products: D)
 392 pyrene (PYR), E) nitropyrene (nitro-PYR), and F) dinitropyrene (dinitro-PYR). Circles represent
 393 observed concentrations. Green circles correspond to urban environments, and blue circles
 394 correspond to non-urban (background/remote) environments.

395

396

397



398

399 **Figure 2.** Box and whisker plot of PAH concentrations for all measurement sites displayed in
 400 Figure 1. Panel A shows concentrations (ng m^{-3}), with red representing the observed data, green
 401 representing the base model simulation, and blue representing simulated PAH concentrations
 402 under the sensitivity simulation (a 90 % reduction in the second order rate coefficients describing
 403 heterogeneous oxidation). The boxes denote the 25th and 75th percentiles, the whiskers denote the
 404 5th and 95th percentiles, the horizontal line denotes the median, and dots denote outliers.
 405 Asterisks (*) indicate where p-value is less than 0.05. Panel B shows the ratio of simulated to
 406 observed PAH concentrations (unitless), with green representing the base, and blue representing
 407 the sensitivity simulation. The 16 directly emitted PAHs considered are naphthalene (NAP),
 408 acenaphthylene (ACY), acenaphthene (ACE), fluorene (FLO), phenanthrene (PHEN), anthracene
 409 (ANT), fluoranthene (FLA), pyrene (PYR), benzo[a]anthracene (BAA), chrysene (CHR),
 410 benzo[b]fluoranthene (BBF), benzo[k]fluoranthene (BKF), benzo[a]pyrene (BAP),
 411 benzo[g,h,i]perylene (BGHIP), indeno[1,2,3-c,d]pyrene (ICDP), and dibenz[a,h]anthracene
 412 (DAHA). Observations are described in greater detail in Materials and Methods, where full
 413 citations are provided.

414

415 We further evaluated model performance at capturing differences in concentrations
 416 between the different PAHs, both globally and in different regions, which are important to
 417 capture the relative cancer risk of different species (not shown). The lighter PAH species are
 418 much more abundant than the heavier species, both globally (Figure 2A) and regionally. The
 419 model generally captures these relative differences in PAH concentrations. Nevertheless, we

420 applied a simple “bias-correction” to the spatial distributions in PAH concentrations to test for
421 the effects of a bias in the differences in concentrations across the different PAHs. Bias
422 correction was conducted by multiplying the simulated PAH concentrations by the average bias
423 between the simulated and observed mean PAH concentration across the non-urban sites (these
424 bias-correction factors are shown in Table S1, SI). These bias-corrected PAH concentration
425 distributions were used in the cancer risk assessment in a sensitivity calculation.

426 To test the ability of the model to simulate the atmospheric lifetime of different PAHs,
427 which affects the composition of PAH mixtures when comparing source and receptor
428 environments, we examined concentration gradients between Central Europe and the Arctic
429 (Figure S1, SI). The model captures the observed PAH concentration gradient between Kocetice
430 (Czech Republic) and Svalbard (Norway) for most of the lighter weight PAH species (ACY,
431 ACE, PHE, ANT, FLA and PYR; Figure S1, SI). The model underpredicts this gradient for
432 heavier PAHs (Figure S1, SI). While uncertainties in lifetimes and emissions combine to
433 influence concentrations at remote sites (Thackray et al., 2015), these biases in lifetime are large
434 enough to offset the likely overestimates in European emissions. To test the importance of these
435 biases, we used the model sensitivity simulation that reduces the second order rate coefficient
436 describing heterogeneous oxidation to 10 % of its original value (‘Het_0.1’). Lighter PAHs are
437 insensitive to changes in heterogeneous oxidation kinetics, as these species exist mostly in the
438 gas-phase. The heavier molecular weight PAHs, which mostly exist in the particle-phase, are
439 extremely sensitive to this sensitivity simulation. Under this simulation where heterogeneous
440 oxidation kinetics are reduced to 10% of the value in the base simulation, the simulated PAH
441 concentration gradients between Kocetice and Svalbard agree with observed values, and biases
442 in PAH concentrations over Svalbard are minimized (Figure S1, SI). We use this sensitivity
443 simulation below to test the influence of uncertainties in heterogeneous oxidation on estimates of
444 human cancer risk (Figure 3 a).

445 For almost all continental regions, PAH concentrations are insensitive to uncertainties in
446 gas-particle partitioning. The poly-parameter linear free energy relationship (ppLFER) gas-
447 particle partitioning scheme used in the base model simulation captures observed particle
448 fractions better than the D&E scheme used in the sensitivity simulation. While particle-phase
449 fractions differed greatly between the two gas-particle partitioning schemes, annual-average
450 PAH concentrations are within 5 % of each other over most continental environments under the
451 two schemes. This is because of the very small differences between simulated gas- and particle-
452 phase lifetimes.

453

454 3.2 Global and Regional Concentrations of PAH Degradation Products

455 We estimated the atmospheric concentrations of N-PAHs (nitro-PAHs and dinitro-PAHs) for all
456 16 of the emitted PAH discussed above (Section 2.4). Within the GEOS-Chem model, the
457 chemical mechanism for pyrene (PYR) accounts for the formation of N-PYR (nitro-PYR and
458 dinitro-PYR) (Table 1). Oxidative processes considered include gas-phase photooxidation (+OH)
459 and direct nitration (+NO₃), and heterogeneous ozonolysis (+O₃) and direct nitration (+NO₃), all
460 of which contribute to N-PYR formation, except heterogeneous ozonolysis. For the remaining N-
461 PAHs, which are not incorporated into the online chemical mechanism, concentrations of the N-

462 PAHs were predicted offline by scaling concentrations of the remaining parent PAHs by
463 spatially resolved ratios of nitro-PYR/PYR and dinitro-PYR/PYR (Figure S2, SI). This approach
464 recognizes that detailed atmospheric degradation data for each individual PAH are not available,
465 and thus provides a bounding estimate of the magnitude of N-PAH impacts under chemically-
466 relevant background conditions. We used sensitivity calculations (described below) to further
467 test the uncertainties introduced by this approach.

468 Simulated global mean atmospheric concentrations of nitro-PYR in the atmosphere are
469 not statistically different from observations ($p < 0.05$, Figure 2B). Spatial patterns in the N-PAHs
470 (nitro-PYR and dinitro-PYR) and the parent PAH, PYR, are very similar (Figure 1D-F). Across
471 non-urban sites, the model underpredicts the observed nitro-PYR concentration (0.016 ng m^{-3}) by
472 a factor of 2.5. This bias is due to a combination of two factors. First, the model underestimates
473 pyrene, the parent compound, by a factor of 1.4, likely due to underestimates of emissions, as
474 described above. Second, our simulated nitro-PYR/PYR ratio of 0.021, is lower (x0.6) than the
475 observed value (0.036) across the aggregated dataset of measurements, implying that we
476 underestimate nitro-PAH formation on average. However, this is not consistent across all
477 environments.

478 We compared the simulated N-PAH/PAH ratio to observed values from field campaigns,
479 which measure the two species simultaneously (Table S2, SI). The simulated nitro-PYR/PYR
480 ratio lies within the range of estimates from field campaigns; our value is x0.2, x0.7 and x3 times
481 the value observed across China, France, Hungary, respectively. These biases vary across the
482 different PAH species, but there were no systematic patterns (Table S2, SI). The simulated nitro-
483 PAH/PAH ratios range from 2.0-4.0 fold of the observed ratios for FLA, 0.2-3.0 fold of the
484 observed ratios for PYR, 0.06-10 fold of the observed ratios for CHR, and 0.02-5.0 fold of the
485 observed ratios for BAP. To account for the impact of potential biases in estimating the cancer
486 risk of PAHs and N-PAHs, we conducted sensitivity calculations by scaling the model-derived
487 N-PAH/PAH ratio by the maximum/minimum bias between the simulated and observed N-
488 PAH/PAH (these scaling factors are shown in Table S2, SI). This provides upper and lower
489 bound estimates for N-PAH formation potential.

490 Heterogeneous direct nitration ($+NO_3$) is the major source of N-PAHs in the atmosphere,
491 as discussed in greater detail in the SI (*Global and Regional Concentrations of PAH*
492 *Degradation Products*). Globally, heterogeneous direct nitration accounts for 99 % of nitro-PYR
493 production in the model. In laboratory studies, this process is a combination of multiple
494 elementary reaction steps. Because the exact mechanism is unknown, we simulated it here using
495 a single-step reaction. Laboratory studies find that the yield of N-PAHs from this process ranges
496 0.04 (Zelenov et al., 2018) – 100 (Ringuet et al., 2012) %. In our model, we assumed a fixed N-
497 PAH formation yield, and chose 100 % in order to bound this reaction pathway; despite this
498 maximal assumption, our model still underestimates the nitro-PYR/PYR ratio as discussed
499 above.

500 The base simulation provides a better representation of the relative importance of parent
501 PAHs and N-PAHs compared to the sensitivity simulation in which heterogeneous oxidation
502 kinetics are reduced to 10 % of their laboratory values. PYR is insensitive to assumptions in
503 heterogeneous oxidation kinetics, as this chemical reaction represents a minor removal term for
504 this species compared with gas-phase oxidation. However, heterogeneous oxidation is the major

505 source of N-PAHs, so as this process slows down, concentrations of N-PAHs reduce. Reductions
506 in the heterogeneous oxidation rate reduce the model's ability to capture the observed N-PYR
507 concentration and N-PYR/PYR ratio (Figure 2B). Hence, while slower oxidation improves
508 reaction kinetics for heavier molecular weight PAHs as discussed above, it decreases the model's
509 ability to capture the observed concentration of N-PYR.

510

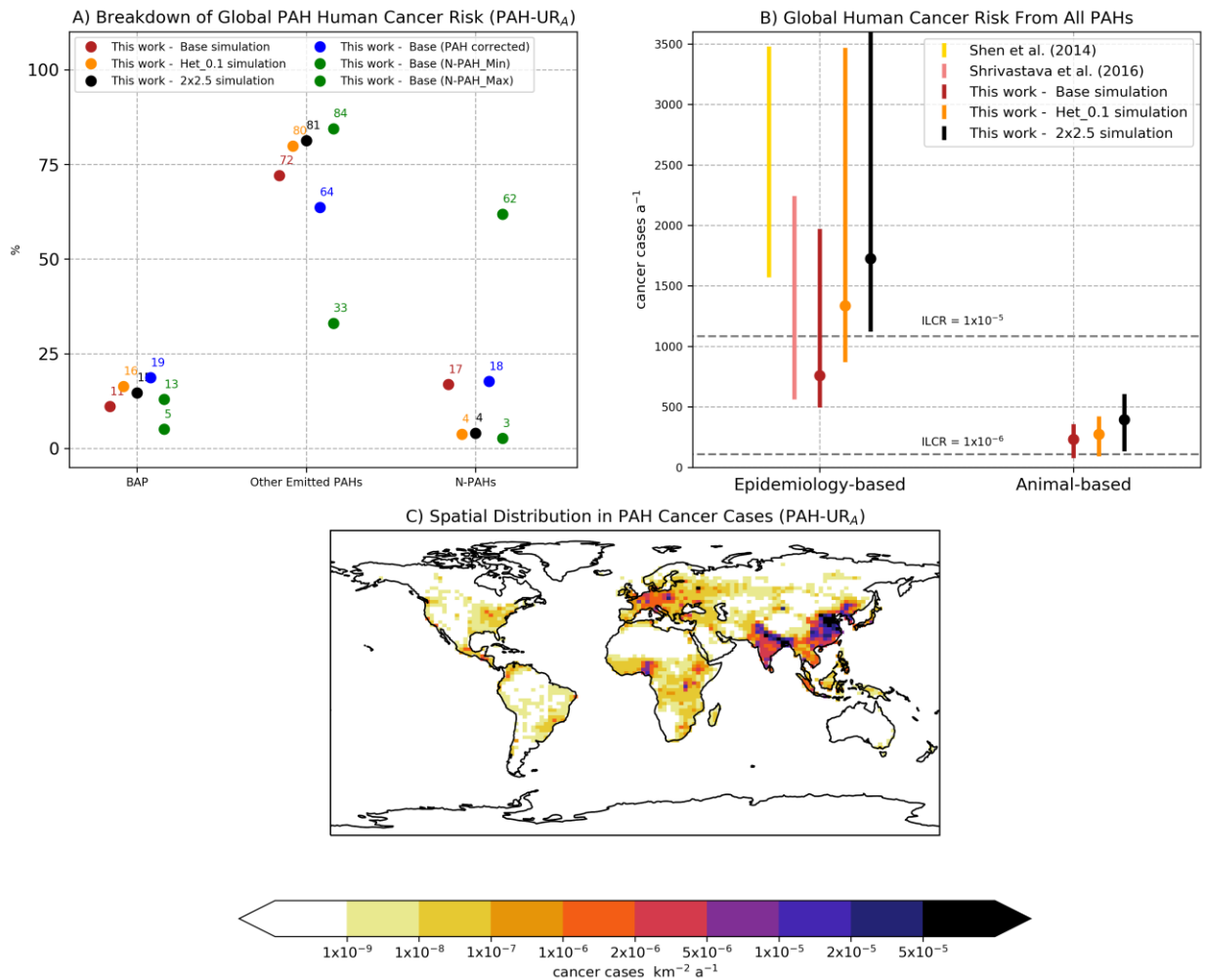
511 3.3 Human Cancer Risk of Ambient PAH Mixtures

512 We calculated the incremental lifetime cancer risk (ILCR) of PAHs (Figure 3) using two
513 different methods (Section 2.6). Briefly, the epidemiologically-based method uses BAP as proxy
514 for risk of the whole PAH mixture, the animal-based method accounts for regional variations in
515 the PAH mixtures.

516 Using the animal-based method allowed us to compare the relative importance of
517 different PAHs to ILCR (Figure 3A). BAP accounts for just 11 % of the calculated global human
518 cancer risk of the entire pollutant mixture, with the remaining emitted PAHs accounting for 72
519 %, and the 12 N-PAHs (6 nitro-PAHs and 6 dinitro-PAHs) for which toxicity information is
520 available account for the remaining 15 % of global ILCR (Figure 3A). The finding that BAP was
521 of low importance to global human cancer risk (11 %) contradicts the findings of previous
522 studies, but was robust across all sensitivity calculations conducted here (5 – 19 %; Figure 3A).
523 Across our sensitivity calculations designed to capture the entire range of observed nitro-
524 PAH/PAH ratios of the 6 PAHs considered, the contribution of N-PAHs to global ILCR ranges
525 from 3-74 % (Figure 3 A). There are very few constraints on the nitro-PAH/PAH ratio; thus, we
526 tested the limits of these values. While these sensitivity calculations gave some indication of the
527 uncertainty related to the importance of N-PAHs, because each calculation used a single field
528 study (i.e. single point) to constrain the entire global distribution of N-PAHs, they should be
529 considered as extreme estimates for the importance of N-PAHs, and only applicable to
530 environments close to where the field study is located. Despite these limitations, our model
531 results suggest that N-PAHs could contribute substantially to global human health, even though
532 they are routinely neglected in risk assessments.

533 Under the animal-based method, PAHs induce a global annual total human lung cancer
534 rate of 231 year⁻¹, which is ~3 times lower than the rate estimated under the epidemiologically-
535 based method (759 year⁻¹, Figure 3B). As noted above, epidemiologically-based methods
536 implicitly address the impacts of mixtures of PAHs, because they are derived from studies in
537 which people were exposed to multiple compounds simultaneously. Our animal-based method
538 results in lower estimates because it includes only a small sample of all known PAHs – the 16
539 emitted species and the N-PAHs for which toxicity information is available. Our animal-based
540 method also does not include other groups of PAHs which may be extremely toxic, such as
541 oxygenated, halogenated and alkylated species (Andersson & Achten, 2015), and assumes that
542 effects of individual PAHs add linearly. Thus, the overall magnitude of ILCR associated with
543 PAHs is likely more realistic using the epidemiologically-based method. However, the
544 epidemiologically-based method does not provide insight as to the toxicity and cancer risk of
545 different chemical species and their respective degradation products. Further, the magnitude and
546 spatial distribution of risk predicted by the epidemiologically-based method are only accurate to

547 the extent that global PAH concentrations reflect the mixtures to which people were exposed in
 548 the original epidemiological studies, and the degree that the overall risk scales with changes in
 549 BAP concentration. Under both methods for estimating ILCR, global ILCR exceeds the
 550 commonly-applied threshold level of 1 in 1,000,000 (1×10^{-6}); this is comparable in magnitude to
 551 estimates from previous studies (Figure 3A). Under the epidemiologically-based method for
 552 estimating human cancer risk of PAHs, 70 (63 - 82) % of the global population breathe air which
 553 exceeds this safe threshold level (with the ranging representing the upper and lower bounds in
 554 BAP toxicity).



555

556 **Figure 3.** Global and regional impacts of ambient PAH concentrations on human cancer risk.
 557 Panel A shows a breakdown in global human cancer risk from different PAHs (%). Panel B
 558 shows global annual cancer rates (cancer cases a⁻¹) induced by PAHs, as estimated by two
 559 different methods (epidemiologically-based, and animal-based), and under three different model
 560 simulations (Base, Het_0.1, and 2x2.5). Estimates from the literature are also shown. Panel C
 561 shows the spatial pattern in PAH-induced human cancer rates under the base simulation,
 562 applying the animal-based method to estimate ILCR (but the pattern is similar for other
 563 formulations, which are not). Note that an ILCR of 1×10^{-6} , applied to the global population

564 ($\sim 7 \times 10^9$) is equal to 7×10^3 lifetime cancer cases, and assuming a life expectancy of 70 years,
565 equates to an annual cancer rate of 100.

566 Under the animal-based method, human cancer risk is much less sensitive to uncertainties
567 in PAH heterogeneous oxidation kinetics than that reported in previous studies using BAP as an
568 indicator species (Shrivastava et al., 2017). This is because when particle-phase PAHs are
569 assumed to be less reactive, concentrations of the parent compounds increase, while
570 concentrations of the oxidation products decrease. Previous studies, which have used the
571 epidemiologically-based method, only accounted for the former (increased human exposure to
572 the parent compound), whereas the animal-based method used here also accounts for the latter
573 (decreased concentrations of the degradation products). Compared to the base simulation (Base =
574 0.19 ng m^{-3}), the global-average population-weighted BAP concentration is 90 % higher in the
575 sensitivity simulation that tests the impact of oxidation kinetics (Het_0.1 = 0.36 ng m^{-3}). Under
576 the epidemiology-based method for estimating ILCR, where the cancer risk of PAHs scale
577 closely with BAP, global ILCR is 76 % higher in the sensitivity simulation (1335 year^{-1})
578 compared to the standard version of the model (759 year^{-1}). However, the animal-based method
579 shows a much weaker sensitivity in global ILCR to particle-phase reactivity. For the same
580 increase in BAP exposure (+ 90 %), the global ILCR increases by only 18 %, from 231 to 273
581 year^{-1} (Figure 3B). Under this method, while slower particle-phase reactivity increases human
582 exposure to the parent compounds, this is partially offset by reductions in exposure to the
583 oxidation products. The animal-based method thus provides a more realistic estimate of the
584 impact of heterogeneous oxidation uncertainty on cancer risks. Human cancer risk is also
585 insensitive to uncertainties in gas-particle partitioning. Both globally and regionally, the ILCR
586 changes by less than 1 % when the gas-particle partitioning scheme is changed from the ppLFER
587 scheme used in the base model simulation, to the D&E scheme used in the sensitivity simulation.
588 Similarly, when the model resolution is increased from $4^\circ \times 5^\circ$ in the base simulation to $2^\circ \times 2.5^\circ$
589 in a sensitivity simulation ('2x2.5'), global ILCR increases by 29 % - however, the relative
590 importance of each PAH species to global ILCR remains unchanged.

591 Although omitted from previous global-scale assessments, uncertainties in BAP toxicity
592 also play a substantial role in influencing the magnitude in global ILCR from PAHs. In Figure
593 3B, for our estimates of global ILCR, the length of the bars represent the uncertainty bounds in
594 BAP toxicity, but for Shen et al. (2014) and Shrivastava et al. (2017), they represent
595 uncertainties associated with genetic susceptibility and heterogeneous oxidation kinetics,
596 respectively. From Figure 3B, under the epidemiologically-based method, uncertainties
597 associated with BAP toxicity (length of red and orange bars in Figure 3B) have a larger influence
598 on global ILCR than uncertainties in genetic susceptibility (lengths of yellow colored bar in
599 Figure 3B) and uncertainties in heterogeneous oxidation kinetics (length of peach colored bar in
600 Figure 3B), highlighting the importance of future research on this parameter.

601 Under the epidemiologically-based and animal-based methods, human cancer risk
602 associated with PAHs is highest in urban and industrial regions, but the two methods differ in
603 their assessments of the spatial variability of these risks. Both methods predict PAH exposure
604 leads to the highest human cancer risk over regions such as China, India, Central and Eastern
605 Europe (Figure 3C). Under the epidemiologically-based method, however, differences in ILCR
606 are driven solely by BAP, whereas under the animal-based method, the ILCR varies spatially
607 with BAP and many other PAHs. When assessing the impact on human cancer risk of reducing

608 BAP emissions (not shown), the epidemiologically-based method would estimate a proportional
609 reduction in the human cancer risk, but the animal-based method would estimate a reduction in
610 human cancer risk a factor of three or more lower (which would vary based on the regional
611 variations in the contribution of BAP to total ILCR).

612

613 **5 Conclusions**

614 We developed and evaluated a new, global-scale model that accounts for 16 emitted PAHs in
615 addition to their degradation products. We used this model to calculate the human cancer risk of
616 exposure to these PAH mixtures using two different methods: an epidemiologically-based
617 method based on BAP concentrations that quantifies overall risk, and an animal-based method
618 that allowed us to attribute risk to individual components of the pollutant mixture without double
619 counting. We then evaluated the relative importance of BAP to global risk, and assessed the
620 utility of using BAP as an indicator compound.

621 We found that BAP is only a small contributor to the global human cancer risk of PAHs
622 (11 %), suggesting it is an inadequate indicator of human cancer risk from this pollutant mixture.
623 Atmospheric modeling studies typically only consider a single PAH species (BAP), and our
624 work suggests that conclusions based on modeling this single compound can be misleading or
625 erroneous. In previous studies, BAP accounted for 40 to 80 % of the cancer risk of PAHs
626 (Delgado-Saborit et al., 2011; Nielsen et al., 1996; Norramit et al., 2005; Zhang et al., 2016;
627 Zhang et al., 2009). However, Zhang et al. (2016) only considered 8 PAHs, which partially
628 explain their high BAP contribution to ILCR over the US ($9-154 \text{ a}^{-1}$) of 40-60 %. In our study,
629 where we considered 16 emitted PAHs and 12 N-PAHs, BAP accounted for 6-15 % of ILCR
630 over the same region. The assumed toxicity of DAHA (ranging from 1-10 times that of BAP),
631 and whether it is even included, varies from study to study. Nielsen et al. (1996), who estimated
632 that BAP accounts for 70% of cancer risk in a field study, did not include DAHA in their
633 analysis. In addition, several highly toxic PAHs were not included in this study, due to lack of
634 data to constrain their emissions and chemistry. Anderson et al. (2015) argues that, in addition to
635 the USEPA16 and N-PAHs, scientific research should be expanded further still, to include other
636 highly toxic parent PAHs and degradation products with an oxy group (O-PAHs). However,
637 atmospheric emission inventories are available only for the USEPA16, and current understanding
638 of O-PAHs is insufficient to build chemical mechanisms within atmospheric models. However,
639 including further PAHs and degradation products would almost certainly further diminish the
640 importance of BAP, strengthening our main conclusions.

641 In addition to the emitted PAHs, we also considered N-PAHs, and we found them to be
642 an important contributor to human cancer risk, but unlike BAP and the other USEPA16, they are
643 not regulated or routinely monitored. Previous assessments of the impact of N-PAHs were
644 limited to a small number of field campaigns and a single box-model study. Our model
645 simulations showed that wherever PAHs are emitted, there is sufficient NO_3 to allow the
646 formation of N-PAHs. Accounting for 15-20 % of the carcinogenic potential of PAH mixtures,
647 we estimated that N-PAHs are comparably dangerous for human cancer risk to BAP (11%). In
648 our sensitivity calculations, the uncertainty in N-PAH/PAH concentration ratios led to
649 considerable variance in the contribution of N-PAH to human cancer risk. Increased confidence

650 in this class of chemical would be provided by (i) a deeper understanding of the formation
651 processes (yields and mechanisms), (ii) a wider understanding of the toxicity of N-PAHs, and
652 (iii) greater geographical coverage and density of observations. Furthermore, in addition to being
653 formed during the oxidation of parent PAHs, as simulated here, N-PAHs can also be directly
654 emitted into the atmosphere. We do not consider direct emissions of N-PAHs in our atmospheric
655 model. Our simulations, however, are constrained by observed values of N-PAHs, thus we
656 believe our result that N-PAHs contribute 15-20 % to global ILCR is a robust bounding estimate.
657 Nevertheless, providing better constraints on the source of N-PAHs in the atmosphere should be
658 a future research priority, especially if mitigation measures are to be considered.

659 PAHs and their degradation products, including N-PAHs, can have a complex impact on
660 human cells, altering transcriptional profiles, signaling networks, and in many cases causing
661 DNA adducts that eventually can progress to DNA mutations. While most research has been
662 focused on understanding the response of cells to single PAH species such as BAP, cancer risk
663 data highlight the need to consider more complex, real-world mixtures of PAHs in order to better
664 define the interactions between different compounds and develop more accurate predictive
665 models.

666 PAHs pose a substantial threat to global human cancer risk across all of our simulations
667 and the two methods for estimating ILCR. We estimated an overall annual cancer risk of 231-
668 759 year⁻¹ from ambient exposure to PAHs globally. Across each of the model simulations and
669 methods in this study, as well as in previous studies, global ILCR exceeded the commonly-
670 applied threshold level of 1 in 1,000,000 (1×10^{-6}) (Figure 3B). Our epidemiologically-based
671 estimate using our base simulation nevertheless calculated a lower global cancer risk than
672 previous studies. Results from Shen et al. (2014) and Shrivastava et al. (2017) are shown for
673 comparison in Figure 3B. Our estimates were lower for three reasons. First, Shen et al. (2014)
674 and Shrivastava et al. (2017) choose to “downscale” their simulated BAP concentrations to
675 reduce bias in urban environments, whereas we did not. Downscaling introduces additional
676 uncertain parameters; we chose instead to apply the best available physical, process-based and
677 explore the importance of simulation biases more directly through supplementary calculations.
678 Second, we used median estimates of the toxicity of BAP, whereas Shen et al. (2014) and
679 Shrivastava et al. (2017) used maximum estimates from the literature. Third, to facilitate
680 comparison of the variability driven by the concentration of different PAHs, we did not account
681 for variability in cancer susceptibility in either of our methods for estimating ILCR, which has
682 been shown to double global ILCR.

683 Our animal-based method provides a more realistic description for spatial differences in
684 the human cancer risk associated with PAHs, as it captures regional differences in PAH
685 mixtures. For example, simulated annual-average BAP concentrations were 3.5 times higher over
686 Hong Kong compared to southern India. Using the epidemiologically-based method, the
687 calculated difference in ILCR between these two locations also differed by the same amount
688 ($\times 3.5$), but the animal-based method suggested that cancer risk in Hong Kong is 12 times higher
689 than over southern India. Hong Kong had a particularly high contribution of DAHA, which the
690 epidemiologically-based method did not account for. This suggests that variations in BAP should
691 not be viewed as indicators of variation in human cancer risk due to PAH mixtures, which is a
692 common conclusion drawn from atmospheric models of BAP alone.

693 While toxicity information used in the animal-based method may not be exactly
694 representative of humans, it does allow us to compare the individual risk of different species in
695 the PAH mixture. PAHs impart their toxic effects on cells through complex pathways that
696 include responses to DNA damage and protein-mediated cellular signaling pathways that alter
697 gene expression of several cytochrome P450s and other enzymes. The expression of PAH-
698 responsive enzymes can vary widely between animals and humans, resulting in differences in
699 susceptibility to these compounds. However, in this study we used literature values of the
700 relative toxicities of PAHs compared to BAP, where mechanisms of action for different PAH
701 species are often similar between animals and humans. There are no human data on the relative
702 toxicities of these PAHs, making us reliant on toxicity data derived from animals where multiple
703 different PAHs have been tested individually in animals. Mechanisms for differences in relative
704 toxicities of PAHs and their nitro derivatives are not yet well understood; however, in most
705 cases, the differences have been attributed to differences in absorption, transport and solubility of
706 compounds in the body (Fu, 1990). More comprehensive understanding of how these
707 pharmacokinetic parameters differ between animal and humans and among different PAH
708 species could further extend the applicability of our animal-based method.

709 In contrast to previous studies, we found that the cancer risks associated with PAHs are
710 not sensitive to uncertainties in heterogeneous oxidation kinetics. As discussed above, when
711 particle-phase PAHs were assumed to be less reactive, concentrations of the parent compounds
712 increase at the expense of concentrations of the oxidation products. Hence, in the animal-based
713 method for estimating human cancer risk, where both emitted PAHs and the degradation
714 products are considered, global ILCR increased by 18 %. Contrastingly, in the
715 epidemiologically-based method for estimating ILCR, which only considers concentrations of a
716 single parent compound (BAP), global ILCR increased by 76 %. This reduced sensitivity
717 contradicts previous results by Shrivastava et al. (2017), who estimated, using an
718 epidemiologically-based method, that reductions in reactivity (due to a hypothesized mechanism
719 including particle shielding) increased global ILCR by a factor of 4, corresponding with five-fold
720 estimates of global-average population-weighted BAP concentration. Hence, our holistic view of
721 PAHs, considering both parent compounds and oxidative derivatives, weakens the sensitivity of
722 PAH human cancer risk to uncertainties in heterogeneous oxidation kinetics. In addition, the
723 human cancer risk associated with PAHs was insensitive to uncertainties in gas-particle
724 partitioning. When then the gas-particle partitioning scheme was changed from the ppLFER to
725 the D&E scheme, global cancer risk changed by less than 1 %.

726 Overall, we conclude that BAP is a poor indicator of human health risks, and that other
727 emitted PAHs and N-PAHs are the dominant contributors to the human cancer risk of PAHs.
728 Researchers and governing bodies should consider extending assessment and monitoring beyond
729 BAP in order to better capture who is affected, and how the health impacts could be mitigated.
730 Increased observations, especially outside North America and Europe, are needed to provide
731 stronger constraints on human exposure to PAHs. We have shown that N-PAHs, which account
732 for only ~1 % of the oxidation products, contribute to human cancer risk. Future research is
733 required to quantify the human health impacts of the remaining PAH degradation products,
734 which will involve a deeper understanding of the chemical mechanisms and kinetics, and the
735 products' toxicity.

736 **Acknowledgments, Samples, and Data**

737 The authors declare no financial conflicts of interests. All data associated with this research is
 738 publicly available. A data directory containing the GEOS-Chem model code, as well as the
 739 python scripts to analysis this code, will be made available in a public repository (likely Zenodo)
 740 upon publication of the peer-reviewed manuscript. We thank John M. Essigmann, Robert Croy,
 741 and Bogdan Fedeles for providing historical context for the toxicological importance of BAP.
 742 We also thank Sebastian D. Eastham for his continued support in running the GEOS-Chem
 743 model. We acknowledge the National Institute of Environmental Health Sciences Superfund
 744 Basic Research Program, National Institute of Health, P42 ES027707, and the MIT Center for
 745 Precision Cancer Medicine. This work was also supported by the University of York's Viking
 746 research computing facility.
 747

748 **References**

- 749
 750
 751 Albinet, A., Leoz-Garziandia, E., Budzinski, H., & Villenave, E. (2007). Polycyclic aromatic
 752 hydrocarbons (PAHs), nitrated PAHs and oxygenated PAHs in ambient air of the
 753 Marseilles area (South of France): Concentrations and sources. *Science of the Total*
 754 *Environment*, 384(1-3), 280-292. doi:10.1016/j.scitotenv.2007.04.028
 755 Amos, H. M., Jacob, D. J., Holmes, C. D., Fisher, J. A., Wang, Q., Yantosca, R. M., . . .
 756 Sunderland, E. M. (2012). Gas-particle partitioning of atmospheric Hg(II) and its effect
 757 on global mercury deposition. *Atmospheric Chemistry and Physics*, 12(1), 591-603.
 758 doi:10.5194/acp-12-591-2012
 759 Andersson, J. T., & Achten, C. (2015). Time to Say Goodbye to the 16 EPA PAHs? Toward an
 760 Up-to-Date Use of PACs for Environmental Purposes. *Polycyclic Aromatic Compounds*,
 761 35(2-4), 330-354. doi:10.1080/10406638.2014.991042
 762 Armstrong, B., Hutchinson, E., Unwin, J., & Fletcher, T. (2004). Lung cancer risk after exposure
 763 to polycyclic aromatic hydrocarbons: A review and meta-analysis. *Environmental Health*
 764 *Perspectives*, 112(9), 970-978. doi:10.1289/ehp.6895
 765 Atkinson, R., Arey, J., Zielinska, B., & Aschmann, S. M. (1990). Kinetics and nitro-products of
 766 the gas-phase OH and NO₃ radical-initiated reactions of naphthalene-d₈, fluoranthene-d₁₀,
 767 and pyrene. *International Journal of Chemical Kinetics*, 22(9), 999-1014.
 768 doi:10.1002/kin.550220910
 769 Bey, I., Jacob, D. J., Yantosca, R. M., Logan, J. A., Field, B. D., Fiore, A. M., . . . Schultz, M. G.
 770 (2001). Global modeling of tropospheric chemistry with assimilated meteorology: Model
 771 description and evaluation. *Journal of Geophysical Research-Atmospheres*, 106(D19),
 772 23073-23095. doi:10.1029/2001jd000807
 773 Bostrom, C. E., Gerde, P., Hanberg, A., Jernstrom, B., Johansson, C., Kyrklund, T., . . .
 774 Westerholm, R. (2002). Cancer risk assessment, indicators, and guidelines for polycyclic
 775 aromatic hydrocarbons in the ambient air. *Environmental Health Perspectives*, 110, 451-
 776 488. doi:10.1289/ehp.02110s3451
 777 Busby, W. F., Stevens, E. K., Martin, C. N., Chow, F. L., & Garner, R. C. (1989). Comparative
 778 lung tumorigenicity of parent and mononitro-polynuclear aromatic-hydrocarbons in the
 779 BLU:Ha newborn mouse assay. *Toxicology and Applied Pharmacology*, 99(3), 555-563.
 780 doi:10.1016/0041-008x(89)90162-2

- 781 Collins, J. F., Brown, J. P., Dawson, S. V., & Marty, M. A. (1991). Risk assessment for benzo[a]
782 pyrene. *Regulatory Toxicology and Pharmacology*, 13(2), 170-184. doi:10.1016/0273-
783 2300(91)90020-v
- 784 Crippa, M., Guizzardi, D., Muntean, M., Schaaf, E., Dentener, F., van Aardenne, J. A., . . .
785 Janssens-Maenhout, G. (2018). Gridded emissions of air pollutants for the period 1970-
786 2012 within EDGAR v4.3.2. *Earth System Science Data*, 10(4), 1987-2013.
787 doi:10.5194/essd-10-1987-2018
- 788 Dachs, J., & Eisenreich, S. J. (2000). Adsorption onto aerosol soot carbon dominates gas-particle
789 partitioning of polycyclic aromatic hydrocarbons. *Environmental Science & Technology*,
790 34(17), 3690-3697. doi:10.1021/es991201+
- 791 Delgado-Saborit, J. M., Stark, C., & Harrison, R. M. (2011). Carcinogenic potential, levels and
792 sources of polycyclic aromatic hydrocarbon mixtures in indoor and outdoor environments
793 and their implications for air quality standards. *Environment International*, 37(2), 383-
794 392. doi:10.1016/j.envint.2010.10.011
- 795 Deutschwenzel, R. P., Brune, H., Grimmer, G., Dettbarn, G., & Misfeld, J. (1983). Experimental
796 studies in rat lungs on the carcinogenicity and dose-response relationships of 8 frequently
797 occurring environmental polycyclic aromatic-hydrocarbons. *Jnci-Journal of the National
798 Cancer Institute*, 71(3), 539-544.
- 799 Dixon, H. M., Armstrong, G., Barton, M., Bergmann, A. J., Bondy, M., Halbleib, M. L., . . .
800 Anderson, K. A. (2019). Discovery of common chemical exposures across three
801 continents using silicone wristbands. *Royal Society Open Science*, 6(2), 19.
802 doi:10.1098/rsos.181836
- 803 Drotikova, T., Ali, A. M., Halse, A. K., Reinardy, H. C., & Kallenborn, R. (2020). Polycyclic
804 aromatic hydrocarbons (PAHs) and oxy- and nitro-PAHs in ambient air of the Arctic
805 town Longyearbyen, Svalbard. *Atmospheric Chemistry and Physics*, 20(16), 9997-10014.
806 doi:10.5194/acp-20-9997-2020
- 807 Eastham, S. D., Weisenstein, D. K., & Barrett, S. R. H. (2014). Development and evaluation of
808 the unified tropospheric-stratospheric chemistry extension (UCX) for the global
809 chemistry-transport model GEOS-Chem. *Atmospheric Environment*, 89, 52-63.
810 doi:10.1016/j.atmosenv.2014.02.001
- 811 Elzein, A., Dunmore, R. E., Ward, M. W., Hamilton, J. F., & Lewis, A. C. (2019). Variability of
812 polycyclic aromatic hydrocarbons and their oxidative derivatives in wintertime Beijing,
813 China. *Atmospheric Chemistry and Physics*, 19(13), 8741-8758. doi:10.5194/acp-19-
814 8741-2019
- 815 Environmental Protection Agency Air Toxics, <https://www.epa.gov/haps> (accessed on
816 September 23, 2020).
- 817 United States Environmental Protection Agency (2009). *Development of a Relative Potency
818 Factor (RPF) Approach for Polycyclic Aromatic Hydrocarbon (PAH) Mixtures
819 (Interagency Science Consultation Draft)*. Retrieved from
820 https://cfpub.epa.gov/si/si_public_record_report.cfm?Lab=NCEA&dirEntryId=194584
821 (accessed on September 23, 2020).
- 822 European Monitoring and Evaluation Programme (EMEP). Retrieved from <https://www.emep.int>
823 (accessed on September 23, 2020).
- 824 Feilberg, A., Kamens, R. M., Strommen, M. R., & Nielsen, T. (1999). Modeling the formation,
825 decay, and partitioning of semivolatile nitro-polycyclic aromatic hydrocarbons

- 826 (nitronaphthalenes) in the atmosphere. *Atmospheric Environment*, 33(8), 1231-1243.
827 doi:10.1016/s1352-2310(98)00275-1
- 828 Fountoukis, C., & Nenes, A. (2007). ISORROPIA II: a computationally efficient thermodynamic
829 equilibrium model for K^+ - Ca^{2+} - Mg^{2+} - $NH_4^{(+)}$ - Na^+ - SO_4^{2-} - NO_3^- - Cl^- - H_2O aerosols.
830 *Atmospheric Chemistry and Physics*, 7(17), 4639-4659. doi:10.5194/acp-7-4639-2007
- 831 Friedman, C. L., Pierce, J. R., & Selin, N. E. (2014). Assessing the Influence of Secondary
832 Organic versus Primary Carbonaceous Aerosols on Long-Range Atmospheric Polycyclic
833 Aromatic Hydrocarbon Transport. *Environmental Science & Technology*, 48(6), 3293-
834 3302. doi:10.1021/es405219r
- 835 Friedman, C. L., & Selin, N. E. (2012). Long-Range Atmospheric Transport of Polycyclic
836 Aromatic Hydrocarbons: A Global 3-D Model Analysis Including Evaluation of Arctic
837 Sources. *Environmental Science & Technology*, 46(17), 9501-9510.
838 doi:10.1021/es301904d
- 839 Friedman, C. L., Zhang, Y. X., & Selin, N. E. (2014). Climate Change and Emissions Impacts on
840 Atmospheric PAH Transport to the Arctic. *Environmental Science & Technology*, 48(1),
841 429-437. doi:10.1021/es403098w
- 842 Fu, P. P. (1990). Metabolism of nitro-polycyclic aromatic-hydrocarbons. *Drug Metabolism*
843 *Reviews*, 22(2-3), 209-268. doi:10.3109/03602539009041085
- 844 Fu, P. P., Von Tungeln, L. S., Chiu, L. H., Zhan, D. J., Deck, J., Bucci, T., & Wang, J. C. (1998).
845 Structure, tumorigenicity, microsomal metabolism, and DNA binding of 7-nitrodibenz
846 a,h anthracene. *Chemical Research in Toxicology*, 11(8), 937-945.
847 doi:10.1021/tx980079+
- 848 GEOS-Chem (wiki page). Retrieved from [http://wiki.seas.harvard.edu/geos-
849 chem/index.php/Main_Page](http://wiki.seas.harvard.edu/geos-chem/index.php/Main_Page) (accessed on September 23, 2020).
- 850 Giglio, L., Randerson, J. T., & van der Werf, G. R. (2013). Analysis of daily, monthly, and
851 annual burned area using the fourth-generation global fire emissions database (GFED4).
852 *Journal of Geophysical Research-Biogeosciences*, 118(1), 317-328.
853 doi:10.1002/jgrg.20042
- 854 Modern-Era Retrospective analysis for Research and Applications Version 2, Global Modeling
855 and Assimilation Office The Modern-Era Retrospective analysis for Research and
856 Applications (Version 2). Retrieved from [https://gmao.gsfc.nasa.gov/reanalysis/MERRA-
857 2/](https://gmao.gsfc.nasa.gov/reanalysis/MERRA-2/) (accessed on September 23, 2020).
- 858 Gray, J. S. (2002). Biomagnification in marine systems: the perspective of an ecologist. *Marine*
859 *Pollution Bulletin*, 45(1-12), 46-52. doi:10.1016/s0025-326x(01)00323-x
- 860 Guenther, A. B., Jiang, X., Heald, C. L., Sakulyanontvittaya, T., Duhl, T., Emmons, L. K., &
861 Wang, X. (2012). The Model of Emissions of Gases and Aerosols from Nature version
862 2.1 (MEGAN2.1): an extended and updated framework for modeling biogenic emissions.
863 *Geoscientific Model Development*, 5(6), 1471-1492. doi:10.5194/gmd-5-1471-2012
- 864 Hansen, T., Seidel, A., & Borlak, J. (2007). The environmental carcinogen 3-nitrobenzanthrone
865 and its main metabolite 3-aminobenzanthrone enhance formation of reactive oxygen
866 intermediates in human A549 lung epithelial cells. *Toxicology and Applied*
867 *Pharmacology*, 221(2), 222-234. doi:10.1016/j.taap.2007.03.003
- 868 Heinrich, U., Roller, M., & Pott, F. (1994). Estimation of a lifetime unit lung-cancer risk for
869 benzo(a)pyrene based on tumor rates in rats exposed to coal tar/pitch condensation
870 aerosol. *Toxicology Letters*, 72(1-3), 155-161. doi:10.1016/0378-4274(94)90023-x

- 871 Hu, L., Millet, D. B., Baasandorj, M., Griffis, T. J., Travis, K. R., Tessum, C. W., . . . de Gouw,
872 J. (2015). Emissions of C-6-C-8 aromatic compounds in the United States: Constraints
873 from tall tower and aircraft measurements. *Journal of Geophysical Research-*
874 *Atmospheres*, 120(2), 826-842. doi:10.1002/2014jd022627
- 875 Keyte, I. J., Harrison, R. M., & Lammel, G. (2013). Chemical reactivity and long-range transport
876 potential of polycyclic aromatic hydrocarbons - a review. *Chemical Society Reviews*,
877 42(24), 9333-9391. doi:10.1039/c3cs60147a
- 878 Klánová, J., Cupr, P., Holoubek, I., Boruvková, J., Přebilová, P., Kareš, R., . . . Ocelka, T.
879 (2008). *Application of passive sampler for monitoring of POPs in ambient air. VI. Pilot*
880 *study for development of the monitoring network in the African continent (MONET-*
881 *AFRICA 2008)*. (Doctoral thesis). Retrieved from author. Location: Masaryk University,
- 882 Koch, R., Knispel, R., Elend, M., Siese, M., & Zetzsch, C. (2007). Consecutive reactions of
883 aromatic-OH adducts with NO, NO₂ and O₂: benzene, naphthalene, toluene, m- and p-
884 xylene, hexamethylbenzene, phenol, m-cresol and aniline. *Atmospheric Chemistry and*
885 *Physics*, 7(8), 2057-2071. doi:10.5194/acp-7-2057-2007
- 886 Lammel, G., Mulder, M. D., Shahpoury, P., Kukucka, P., Liskova, H., Pribylova, P., . . .
887 Wotawa, G. (2017). Nitro-polycyclic aromatic hydrocarbons - gas-particle partitioning,
888 mass size distribution, and formation along transport in marine and continental
889 background air. *Atmospheric Chemistry and Physics*, 17(10), 6257-6270.
890 doi:10.5194/acp-17-6257-2017
- 891 Lammel, G., Sehili, A. M., Bond, T. C., Feichter, J., & Grassl, H. (2009). Gas/particle
892 partitioning and global distribution of polycyclic aromatic hydrocarbons - A modelling
893 approach. *Chemosphere*, 76(1), 98-106. doi:10.1016/j.chemosphere.2009.02.017
- 894 Liu, C. G., Zhang, P., Yang, B., Wang, Y. F., & Shu, J. N. (2012). Kinetic Studies of
895 Heterogeneous Reactions of Polycyclic Aromatic Hydrocarbon Aerosols with NO₃
896 Radicals. *Environmental Science & Technology*, 46(14), 7575-7580.
897 doi:10.1021/es301403d
- 898 Ma, Y. X., Xie, Z. Y., Yang, H. Z., Moller, A., Halsall, C., Cai, M. H., . . . Ebinghaus, R. (2013).
899 Deposition of polycyclic aromatic hydrocarbons in the North Pacific and the Arctic.
900 *Journal of Geophysical Research-Atmospheres*, 118(11), 5822-5829.
901 doi:10.1002/jgrd.50473
- 902 Miet, K., Le Menach, K., Flaud, P. M., Budzinski, H., & Villenave, E. (2009). Heterogeneous
903 reactions of ozone with pyrene, 1-hydroxypyrene and 1-nitropyrene adsorbed on
904 particles. *Atmospheric Environment*, 43(24), 3699-3707.
905 doi:10.1016/j.atmosenv.2009.04.032
- 906 Moolgavkar, S. H., Luebeck, E. G., & Anderson, E. L. (1998). Estimation of unit risk for coke
907 oven emissions. *Risk Analysis*, 18(6), 813-825. doi:10.1111/j.1539-6924.1998.tb01124.x
- 908 Mu, Q., Shiraiwa, M., Octaviani, M., Ma, N., Ding, A. J., Su, H., . . . Cheng, Y. F. (2018).
909 Temperature effect on phase state and reactivity controls atmospheric multiphase
910 chemistry and transport of PAHs. *Science Advances*, 4(3). doi:10.1126/sciadv.aap7314
- 911 Mulder, M. D., Dumanoglu, Y., Efstathiou, C., Kukucka, P., Matejovicova, J., Maurer, C., . . .
912 Lammel, G. (2019). Fast Formation of Nitro-PAHs in the Marine Atmosphere
913 Constrained in a Regional-Scale Lagrangian Field Experiment. *Environmental Science &*
914 *Technology*, 53(15), 8914-8924. doi:10.1021/acs.est.9b03090
- 915 Nielsen, T., Jorgensen, H. E., Larsen, J. C., & Poulsen, M. (1996). City air pollution of
916 polycyclic aromatic hydrocarbons and other mutagens: Occurrence, sources and health

- 917 effects. *Science of the Total Environment*, 189, 41-49. doi:10.1016/0048-9697(96)05189-
918 3
- 919 Nisbet, I. C. T., & Lagoy, P. K. (1992). Toxic equivalency factors (TEFs) for polycyclic
920 aromatic-hydrocarbons (PAHS). *Regulatory Toxicology and Pharmacology*, 16(3), 290-
921 300. doi:10.1016/0273-2300(92)90009-x
- 922 Norramit, P., Cheevaporn, V., Itoh, N., & Tanaka, K. (2005). Characterization and carcinogenic
923 risk assessment of polycyclic aromatic hydrocarbons in the respirable fraction of airborne
924 particles in the Bangkok Metropolitan area. *Journal of Health Science*, 51(4), 437-446.
925 doi:10.1248/jhs.51.437
- 926 Norwegian Institute for Air Research. Retrieved from <http://ebas.nilu.no> (accessed on September
927 23, 2020).
- 928 Octayiani, M., Tost, H., & Lammel, G. (2019). Global simulation of semivolatile organic
929 compounds - development and evaluation of the MESSy submodel SVOC (v1.0).
930 *Geoscientific Model Development*, 12(8), 3585-3607. doi:10.5194/gmd-12-3585-2019
- 931 Park, E. J., & Park, K. (2009). Induction of pro-inflammatory signals by 1-nitropyrene in
932 cultured BEAS-2B cells. *Toxicology Letters*, 184(2), 126-133.
933 doi:10.1016/j.toxlet.2008.10.028
- 934 Perraudin, E., Budzinski, H., & Villenave, E. (2007). Kinetic study of the reactions of ozone with
935 polycyclic aromatic hydrocarbons adsorbed on atmospheric model particles. *Journal of*
936 *Atmospheric Chemistry*, 56(1), 57-82. doi:10.1007/s10874-006-9042-x
- 937 Poschl, U., Letzel, T., Schauer, C., & Niessner, R. (2001). Interaction of ozone and water vapor
938 with spark discharge soot aerosol particles coated with benzo a pyrene: O₃ and H₂O
939 adsorption, benzo a pyrene degradation, and atmospheric implications. *Journal of*
940 *Physical Chemistry A*, 105(16), 4029-4041. doi:10.1021/jp004137n
- 941 Ringuet, J., Albinet, A., Leoz-Garziandia, E., Budzinski, H., & Villenave, E. (2012). Reactivity
942 of polycyclic aromatic compounds (PAHs, NPAHs and OPAHs) adsorbed on natural
943 aerosol particles exposed to atmospheric oxidants. *Atmospheric Environment*, 61, 15-22.
944 doi:10.1016/j.atmosenv.2012.07.025
- 945 Saha, M., Maharana, D., Kurumisawa, R., Takada, H., Yeo, B. G., Rodrigues, A. C., . . . Viet, P.
946 H. (2017). Seasonal Trends of Atmospheric PAHs in Five Asian Megacities and Source
947 Detection Using Suitable Biomarkers. *Aerosol and Air Quality Research*, 17(9), 2247-
948 2262. doi:10.4209/aaqr.2017.05.0163
- 949 Sander, R. (2015). Compilation of Henry's law constants (version 4.0) for water as solvent.
950 *Atmospheric Chemistry and Physics*, 15(8), 4399-4981. doi:10.5194/acp-15-4399-2015
- 951 Shahpoury, P., Lammel, G., Albinet, A., Sofuoglu, A., Dumanoglu, Y., Sofuoglu, S. C., . . .
952 Zdimal, V. (2016). Evaluation of a Conceptual Model for Gas-Particle Partitioning of
953 Polycyclic Aromatic Hydrocarbons Using Polyparameter Linear Free Energy
954 Relationships. *Environmental Science & Technology*, 50(22), 12312-12319.
955 doi:10.1021/acs.est.6b02158
- 956 Shen, H. Z., Huang, Y., Wang, R., Zhu, D., Li, W., Shen, G. F., . . . Tao, S. (2013). Global
957 Atmospheric Emissions of Polycyclic Aromatic Hydrocarbons from 1960 to 2008 and
958 Future Predictions. *Environmental Science & Technology*, 47(12), 6415-6424.
959 doi:10.1021/es400857z
- 960 Shen, H. Z., Tao, S., Liu, J. F., Huang, Y., Chen, H., Li, W., . . . Liu, W. X. (2014). Global lung
961 cancer risk from PAH exposure highly depends on emission sources and individual
962 susceptibility. *Scientific Reports*, 4. doi:10.1038/srep06561

- 963 Shrivastava, M., Lou, S., Zelenyuk, A., Easter, R. C., Corley, R. A., Thrall, B. D., . . . Tao, S.
964 (2017). Global long-range transport and lung cancer risk from polycyclic aromatic
965 hydrocarbons shielded by coatings of organic aerosol. *Proceedings of the National*
966 *Academy of Sciences of the United States of America*, 114(6), 1246-1251.
967 doi:10.1073/pnas.1618475114
- 968 Socioeconomic Data and Applications Center (SEDAC). Retrieved from
969 <https://sedac.ciesin.columbia.edu> (accessed on September 23, 2020).
- 970 Thackray, C. P., Friedman, C. L., Zhang, Y. X., & Selin, N. E. (2015). Quantitative Assessment
971 of Parametric Uncertainty in Northern Hemisphere PAH Concentrations. *Environmental*
972 *Science & Technology*, 49(15), 9185-9193. doi:10.1021/acs.est.5b01823
- 973 Thyssen, J., Althoff, J., Kimmerle, G., & Mohr, U. (1981). Inhalation studies with benzo[a]
974 pyrene in syrian golden-hamsters. *Journal of the National Cancer Institute*, 66(3), 575-
975 577.
- 976 Travis, K. R., Jacob, D. J., Fisher, J. A., Kim, P. S., Marais, E. A., Zhu, L., . . . Zhou, X. L.
977 (2016). Why do models overestimate surface ozone in the Southeast United States?
978 *Atmospheric Chemistry and Physics*, 16(21), 13561-13577. doi:10.5194/acp-16-13561-
979 2016
- 980 van Donkelaar, A., Martin, R. V., Leaitch, W. R., Macdonald, A. M., Walker, T. W., Streets, D.
981 G., . . . Andreae, M. O. (2008). Analysis of aircraft and satellite measurements from the
982 Intercontinental Chemical Transport Experiment (INTEX-B) to quantify long-range
983 transport of East Asian sulfur to Canada. *Atmospheric Chemistry and Physics*, 8(11),
984 2999-3014. doi:10.5194/acp-8-2999-2008
- 985 Wesely, M. L. (1989). Parameterization of surface resistances to gaseous dry deposition in
986 regional-scale numerical-models. *Atmospheric Environment*, 23(6), 1293-1304.
987 doi:10.1016/0004-6981(89)90153-4
- 988 Wilson, J. (2020). Modeling the Formation, Degradation, and Spatiotemporal Distribution of 2-
989 Nitrofluoranthene in the Global Atmosphere. *Environ Sci Technol* 54, 14224–14234.
- 990 Wislocki, P. G., Bagan, E. S., Lu, A. Y. H., Dooley, K. L., Fu, P. P., Hanhsu, H., . . . Kadlubar,
991 F. F. (1986). Tumorigenicity of nitrated derivatives of pyrene, benz[a]anthracene,
992 chrysene and benzo[a]pyrene in the newborn mouse assay. *Carcinogenesis*, 7(8), 1317-
993 1322. doi:10.1093/carcin/7.8.1317
- 994 Zelenov, V. V., Aparina, E. V., Kozlovskiy, V. I., Sulimenkov, I. V., & Nosyrev, A. E. (2018).
995 Kinetics of NO₃ Uptake on Pyrene as a Representative Organic Aerosols. *Russian*
996 *Journal of Physical Chemistry B*, 12(2), 343-351. doi:10.1134/s1990793118020136
- 997 Zhang, J., Li, J. Y., Wang, P., Chen, G., Mendola, P., Sherman, S., & Ying, Q. (2017).
998 Estimating population exposure to ambient polycyclic aromatic hydrocarbon in the
999 United States - Part I: Model development and evaluation. *Environment International*, 99,
1000 263-274. doi:10.1016/j.envint.2016.12.002
- 1001 Zhang, J., Wang, P., Li, J. Y., Mendola, P., Sherman, S., & Ying, Q. (2016). Estimating
1002 population exposure to ambient polycyclic aromatic hydrocarbon in the United States -
1003 Part II: Source apportionment and cancer risk assessment. *Environment International*, 97,
1004 163-170. doi:10.1016/j.envint.2016.08.024
- 1005 Zhang, L. M., Gong, S. L., Padro, J., & Barrie, L. (2001). A size-segregated particle dry
1006 deposition scheme for an atmospheric aerosol module. *Atmospheric Environment*, 35(3),
1007 549-560. doi:10.1016/s1352-2310(00)00326-5

- 1008 Zhang, P., Sun, W. Q., Li, N. N., Wang, Y. F., Shu, J. N., Yang, B., & Dong, L. (2014). Effects
1009 of Humidity and $\text{NO}_3/\text{N}_2\text{O}_5$ Ratio on the Heterogeneous Reaction of Fluoranthene and
1010 Pyrene with $\text{N}_2\text{O}_5/\text{NO}_3/\text{NO}_2$. *Environmental Science & Technology*, 48(22), 13130-
1011 13137. doi:10.1021/es504508v
- 1012 Zhang, Y. X., Tao, S., Shen, H. Z., & Ma, J. M. (2009). Inhalation exposure to ambient
1013 polycyclic aromatic hydrocarbons and lung cancer risk of Chinese population.
1014 *Proceedings of the National Academy of Sciences of the United States of America*,
1015 106(50), 21063-21067. doi:10.1073/pnas.0905756106
- 1016 Zhou, S., Hwang, B. C. H., Lakey, P. S. J., Zuend, A., Abbatt, J. P. D., & Shiraiwa, M. (2019).
1017 Multiphase reactivity of polycyclic aromatic hydrocarbons is driven by phase separation
1018 and diffusion limitations. *Proceedings of the National Academy of Sciences of the United*
1019 *States of America*, 116(24), 11658-11663. doi:10.1073/pnas.1902517116
- 1020 Zhou, S. M., Shiraiwa, M., McWhinney, R. D., Poschl, U., & Abbatt, J. P. D. (2013). Kinetic
1021 limitations in gas-particle reactions arising from slow diffusion in secondary organic
1022 aerosol. *Faraday Discussions*, 165, 391-406. doi:10.1039/c3fd00030c
- 1023
1024